Joint Coordination Control of Hybrid Energy Storage System in New Distribution Network

Hao Bai[1,*], Qingsheng Li[2], Yuxin Wen[1] and Yipeng Liu[1]

[1]*Electric Power Research Institute, CSG, Guangzhou 510663, Guangdong, China*
[2]*Guizhou Power Grid Co., Ltd. Power Grid Planning and Research Center Ltd, Guiyang 510003, Guizhou, China*
E-mail: j6k3an@163.com
[*]*Corresponding Author*

Received 17 November 2025; Accepted 17 December 2025

Abstract

The current mixed energy storage (ES) system in the distribution network (DN) has become the main power system for new energy construction, but how to achieve joint optimization control of the mixed energy system in the DN is still the focus of current research. To achieve joint coordinated control of hybrid ES systems in new DNs, this study introduces a coordinated control model for ES systems based on multi-objective optimization (MOO) algorithms. The new model uses MOO algorithms to coordinate and optimize the ES system in the DN, thereby achieving accurate coordinated control of the ES system. The results show that using MOO algorithms, the network loss of the hybrid ES system is reduced by 1.258 MW, and the load disturbance

Strategic Planning for Energy and the Environment, Vol. 45_2, 321–348.
doi: 10.13052/spee1048-5236.4522

was reduced by 0.24. At the same time, after using the new method, the operating cost of the hybrid ES system is reduced by about 40,000 yuan/year, and the grid losses of nodes are reduced by about 8.65%. The joint coordinated control method of the new ES system can improve the ES optimization effect of the system and reduce ES losses in the power grid. This study has good guiding significance for improving the ES efficiency of new DNs.

Keywords: New type of distribution network, hybrid energy storage system, multi-objective optimization, coordinated control.

1 Introduction

With the acceleration of the global energy transition, high proportions of renewable energy (RE), represented by photovoltaics and wind power, are being connected to the distribution network (DN) on a large scale [1, 2]. However, the integration of high proportions of RE sources has intensified bidirectional power flows within DNs, resulting in significant intraday power fluctuations and voltage overshoot risks. Concurrently, the phenomenon of curtailed wind and solar power generation has led to substantial wastage of clean energy resources [3, 4]. As a key mechanism for smoothing fluctuations, supporting voltage, and accommodating curtailed electricity, hybrid energy storage systems face significant challenges in coordinating control between storage units with differing characteristics (such as power-type electrochemical storage and energy-type hydrogen storage). These challenges primarily manifest in the complexity of multi-timescale power allocation, the inherent conflict between economic objectives (investment and operational costs) and technical objectives (voltage quality, grid losses), and the coupled impact of equipment lifetime degradation and long-term system operating costs [5, 6]. Gu T et al. proposed a new collaborative control method. This method establishes a multi-objective model for enhancing the layout and capacity of battery ES systems and improves the non-dominated sorting genetic algorithm (NSGA) by increasing the selection coefficient of the optimal solution (OS) of the population. Experiments showed that this method was effective and superior in IEEE 33 nodes [7]. To tackle the challenge of energy imbalance in the DN caused by distributed generation access, Liu K proposed a new source-load-storage collaborative scheduling method. This method first constructs a system model consisting of a DN and a source-load-storage system, integrates Adaboost ensemble CNN and BiLSTM for

load-side fluctuation prediction, and uses a multi-objective sparrow search algorithm to solve the system. Experiments showed that this method could effectively solve the optimal scheduling problem of distributed generation access [8]. Shafiei K et al. proposed a new multi-objective optimization (MOO) control model to improve the grid resilience of the integration of new energy (NE) generation and battery ES systems. This model examines the correlation between battery relative capacity and the total cost of the system, and designs a demand response program to manage multiple types of loads to achieve the optimization objective. Experiments showed that this model reduced the total load of the system by 40%, and optimizing the battery capacity could significantly reduce the total cost [9]. Piltan G et al. introduced a new collaborative control method to optimize the elastic operation capability of smart DNs with NE virtual power plants. This method uses a hybrid stochastic-robust strategy to model the accessibility of smart DN equipment and the uncertainty of NE virtual power plants, and combines the krill swarm optimization algorithm with the sine and cosine algorithms. Experiments showed that the standard deviation of this method in IEEE 69 was 0.93%, and the system resilience was improved by 95% [10]. Abid MS et al. proposed a new artificial hummingbird algorithm optimization method for the planning optimization problem of distributed NE power generation (PG). The method aims to minimize voltage deviation and save annual economy. It uses probability distribution function to evaluate the fuzziness related to the randomness of photovoltaic and wind power output power. Experiments showed that the artificial hummingbird algorithm had better optimization efficiency than the improved Harris Eagle fusion particle swarm optimization (PSO) algorithm, [11]. Zadehbagheri M et al. introduced a new bi-objective optimization model for the layout optimization problem of virtual power plants under adverse conditions. The model uses the Pareto optimization strategy based on the ε-constraint approach to realize the single objective formula. It employs a solver that leverages the Crow search algorithm along with the sine and cosine algorithm to secure a dependable OS, characterized by minimal dispersion in the final outcome. Experiments showed that the model proved its ability to boost the economic performance, usage efficiency, and robustness of the DN in the IEEE 69 system [12]. Pompern N et al. introduced a novel MOO model. The model considers the minimization of system cost, transmission loss and voltage stability, and uses PSO algorithm and salt swarm algorithm to solve the problems. Experiments showed that the Improved PSO (IMPSO) algorithm provided the best objective value and

the salt swarm algorithm provided the fastest return cycle, resulting in stable system voltage, reduced transmission loss and reduced peak demand [13].

In summary, existing research has explored joint optimization methods for energy storage systems when integrating new energy sources into distribution grids from multiple perspectives. However, the following limitations remain: (1) Most studies treat capacity planning and operational control as separate entities, lacking a comprehensive joint optimization framework spanning the entire lifecycle from planning to operation. (2) Optimization models predominantly focus on traditional economic and technical requirements, with insufficient characterization of carbon trading costs and equipment lifecycle costs under the dual carbon goals. (3) Solution algorithms frequently encounter challenges of slow convergence or susceptibility to local optima when addressing high-dimensional, non-linear, multi-constraint joint optimization problems. Therefore, this study introduces a hybrid multi-objective joint optimization model integrating capacity configuration and operation control, aiming to improve grid stability and reliability and foster the high-quality development of new power systems. The core innovation of this research lies in: (1) Model Innovation: Proposing an integrated 'planning-operation' joint optimization framework that simultaneously incorporates stepwise carbon trading costs and lifecycle-accounting equipment renewal costs into a multi-objective optimization model for hybrid energy storage. This ensures optimization outcomes better align with practical economic viability and sustainability requirements under the dual carbon goals. (2) Algorithm Innovation: Addressing the high-dimensional complexity of the joint optimization model by innovatively integrating the Carnivorous Plant Algorithm (CPA) with the Longhorn Beetle Search-Improved Particle Swarm Hybrid Algorithm (BAS-IMPSO). Algorithmic Innovation: Addressing the high-dimensional complexity of the joint optimization model, it innovatively integrates the CPA with the BAS-IMPSO hybrid algorithm. CPA tackles the planning-layer capacity optimization problem with its robust global search capability, while BAS-IMPSO addresses the operational-layer real-time power allocation issue, combining global exploration with local fine-tuning. This hybrid strategy effectively enhances solution efficiency and solution set quality for complex problems. (3) Strategy Innovation: A multi-mode adaptive coordination control strategy is designed, considering the difference between new energy output and load demand. Based on power surplus/deficit conditions, it dynamically adjusts the charging/discharging priority of battery energy storage and hydrogen storage to achieve optimal internal energy consumption.

2 Coordinated Optimization Control of ES System in DN

2.1 Capacity Optimization of Hybrid ES System in DN

To get rid of the over-reliance on non-RE, reduce environmental pollution, and accelerate energy transformation, the scale of NE PG (such as photovoltaic and wind power) has been expanding [14]. Although NE power has multiple advantages such as being clean and environmentally friendly, enhancing local power supply resilience and alleviating grid investment pressure, its intermittency, volatility, uncontrollability, and the problem of wind and solar curtailment exert a notable influence on grid stability. ES system is the core to solving the above problems of NE DN. It can realize energy time shift by peak shaving and valley filling, thereby smoothing voltage fluctuations in DN and improving power quality. The study proposes a joint coordination control framework, first optimizing the capacity of the hybrid ES system in the DN at the planning level, and then controlling the operation of the hybrid ES system in the DN at the operation level. Capacity configuration provides the physical basis and constraints for operation control, while operation strategy and performance feedback guide and verify capacity planning, forming a closed-loop joint optimization system. The application of ES system in NE DN is shown in Figure 1.

In Figure 1, ES systems typically employ electrochemical ES or lithium battery ES. The distributed arrangement of ES systems enables local consumption and balance of electrical energy, rapid response, and reduced transmission losses. ES systems are mainly located near power sources,

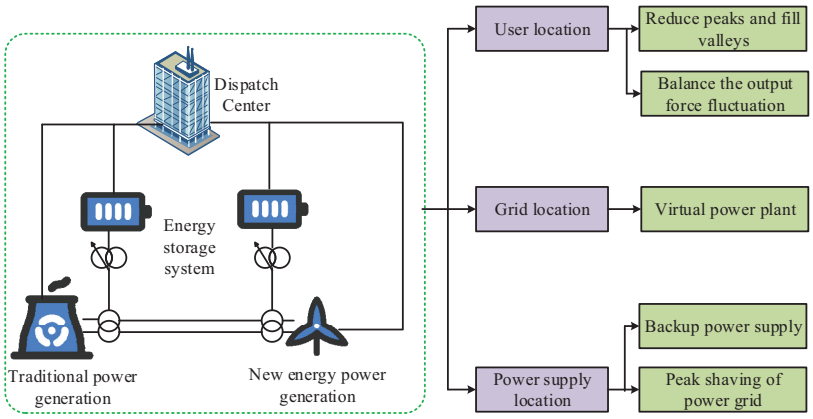

Figure 1 Application of ES systems in NE DNs.

power grids, and users. At the power grid, they can improve grid security, stability, and economy; at the power source, they can increase PG revenue and meet grid connection requirements; and at the user, they can reduce electricity costs and ensure power supply reliability. The capacity optimization of the hybrid ES system in the DN selects three indicators as objective functions (OFs): economy, voltage quality, and system loss, and the calculation is shown in Equation (1) [15].

$$\min F = \min f_1 + \min f_2 + \min f_3 \tag{1}$$

In Equation (1), F is the overall OF, f_1 is the economic objective, f_2 is the voltage quality objective, and f_3 is the system loss objective. The economic objective is divided into initial investment cost and subsequent benefits, and is calculated as shown in Equation (2).

$$\min C_U = \sum_{i=1}^{k} E_s \cdot c_{ba} + P_s \cdot c_{in} + E_s \cdot c_{inst} + c_{fixde} + \sum_{i=1}^{k} c_i P_s \tag{2}$$

In Equation (2), C_U is the initial investment cost, k is the total number of ES systems, E_s is the rated capacity of the ES system, c_{ba} is the unit cost of the ES battery, and P_s is the rated power of the ES system. c_{in} is the unit cost of the inverter, c_{inst} is the installation cost of the ES system, and c_{fixde} is the fixed costs such as design fees. c_i is the maintenance cost of the ith ES system. Subsequent revenue includes peak shaving and valley filling revenue and government subsidy revenue, calculated as shown in Equation (3) [16].

$$\min C_L = \sum_{t=1}^{T} \alpha_t \cdot P_t \cdot \Delta t + \sum_{i=1}^{k} \sum_{t=1}^{T} \beta P_i \Delta t \tag{3}$$

In Equation (3), C_L is the later-stage revenue, α_t is the electricity price at time t, P_t is the power at the point of sale and purchase of the ES system and the DN at time t, Δt is the time interval, T is the operating cycle, which is generally 24 hours. β is the government subsidy unit price, and P_i is the discharge power of the ith ES system. $\min f_1 = \min C_U + \min C_L$. The voltage quality index is calculated as shown in Equation (4).

$$\min f_2 = \sum_{j=1}^{K} \sum_{t=1}^{T} |U_{t,j} - 1| \tag{4}$$

In Equation (4), K is the total amount of nodes in the DN, and $U_{t,j}$ is the voltage amplitude of the node j at time t. The system loss index is calculated as presented in Equation (5).

$$\min f_3 = \sum_{j=1}^{K} \sum_{t=1}^{T} \frac{P_{t,j}^2 \cdot R_j}{U_{t,j}^2 \cdot \cos^2 \delta} \Delta t \alpha_t \tag{5}$$

In Equation (5), $P_{t,j}$ is the active power of node j at time t, R_j is the resistance of the node j, $U_{t,j}$ is the voltage of node j at time t, and δ is the power factor angle. Because the dimensions of different OFs differ significantly, a normalization process is performed. The normalized OF is $F_i = \frac{\max f_i - f_i}{\max f_i - \min f_i}$, where F_i is the processed OF, and f_i is the ith OF. The hybrid ES system of the DN must achieve active power balance and ensure that the load consumption probability plus network loss power equals the PG plus or minus the ES battery power at each time point. The calculation of the charging and discharging constraints of the ES battery is shown in Equation (6).

$$\begin{cases} Q_{\min}^i \leq Q_i \leq Q_{\max}^i \\ P_{i,t} \leq P_i \end{cases} \tag{6}$$

In Equation (6), Q_i is the state of charge (SOC) of the ES battery i, $Q_{\min}^i$ is the min SOC, $Q_{\max}^i$ is the max SOC, $P_{i,t}$ is the operating power of the battery i at time t, and P_i is the max power of the battery i. The weighting coefficients are determined using the Analytic Hierarchy Process (AHP). A pairwise comparison judgement matrix was first constructed for the three factors: economic efficiency, voltage quality, and system losses. Domain experts were invited to assign scores, and after calculating the eigenvectors and performing consistency checks (CR < 0.1), the aforementioned weights were obtained. This weighting allocation reflects the decision-making preference in current DN operations, where economic efficiency is the primary consideration, followed by voltage quality, with system losses being relatively important. Following comprehensive calculation, the weighting coefficients for the three objective functions were determined as 0.540, 0.297, and 0.163 respectively. Since the optimization model of the hybrid ES system of the DN has multi-dimensional and complex problems, the existing solution method is slow and cannot ensure the global OS. The CPA is employed for capacity optimization, as its mechanism simulating ecological competition demonstrates exceptional global exploration capabilities and convergence speed (CS) when solving high-dimensional, non-convex capacity allocation

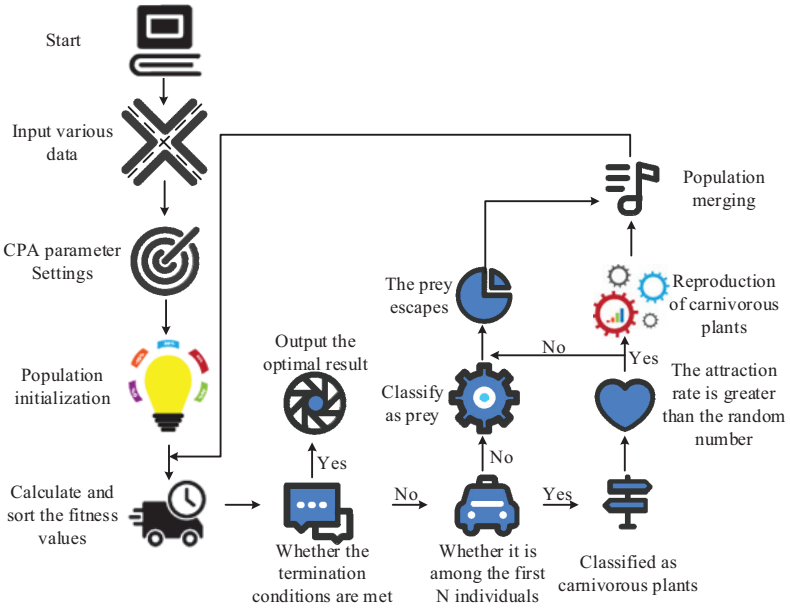

Figure 2 Specific structure of the CPA.

problems. It is well-suited for addressing combinatorial optimization problems involving discrete variables, such as the location of energy storage installations. Therefore, the study uses the CPA to solve the model. This algorithm solves the complex optimization problem by simulating the strategy of carnivorous plants (such as Venus flytraps, pitcher plants, etc.) to attract, capture and digest prey [17]. The CPA has a strong global exploration and local development balancing ability, fewer parameters and fast CS. The specific structure of the CPA is shown in Figure 2.

In Figure 2, the relevant data of the power DN and ES system are first input, and the CPA parameters are set to initialize the population. The fitness values of individuals are calculated and sorted in ascending order. It is then determined whether the population fitness values meet the termination condition; if so, the OS is output. If not, the individuals with the highest fitness values are classified as carnivorous plants, and the remaining individuals are classified as prey. An attraction rate is set for prey. When the prey attraction rate is greater than a random number, the prey moves towards the carnivorous plants, which then prey on and digest the prey, reproducing into new carnivorous plants. When the prey attraction rate falls below a random number, the prey continues to grow. Escaped prey form new populations with

carnivorous plants, and fitness values are recalculated until the maximum iteration count is reached.

2.2 Operation Control of Hybrid ES System in DN

Although electrochemical ES has high energy efficiency, its equipment lifespan is limited, and the amount of electricity it can store will decrease significantly in the later stages of operation. While hydrogen ES has an energy efficiency of only 30%–40%, its ES capacity can reach the megawatt level, and its equipment lifespan is also longer [18]. Therefore, this study proposes to use the two ES methods in combination to solve the contradictions between efficiency and scale, and between short-term and long-term needs that cannot be overcome by a single ES technology, and to achieve a high proportion of RE access to the DN. At the same time, the power distribution between the battery and hydrogen ES is dynamically managed according to the real-time operating conditions, and coordinated control is performed within the capacity limits defined by the planning layer [19]. The specific structure of the hybrid ES system for the DN is shown in Figure 3.

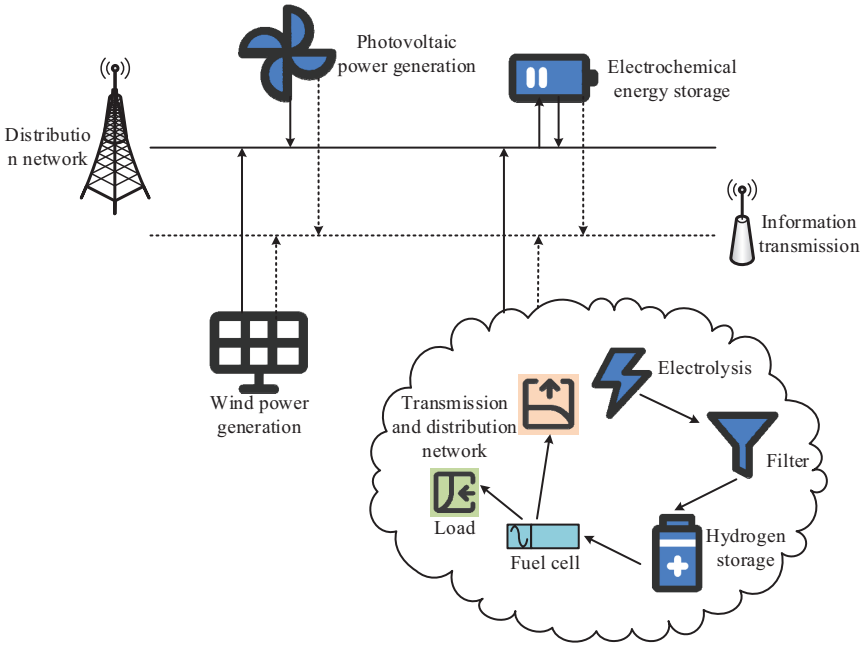

Figure 3 Specific structure of hybrid ES system in DNs.

In Figure 3, the hybrid ES system of the power DN includes traditional energy PG (thermal power, nuclear power, hydropower) and NE PG (wind power, photovoltaic power, geothermal power) at the PG end. The power at the PG end is directly connected to the power DN and ES equipment. The hydrogen ES battery is mainly used to provide power to guarantee the stability of the power DN during the peak electricity consumption period at night when the energy of the electrochemical ES battery is exhausted. When the power is surplus, water is electrolyzed into hydrogen and oxygen in the electrolyzer, and the generated hydrogen is purified and compressed and stored in the hydrogen storage tank. When the power is short, hydrogen is burned in the fuel cell to generate electricity and input into the power DN. At the same time, according to the tiered carbon trading policy, the study introduces it into an MOO model to further reduce the carbon emissions of the system. The model mainly considers the economic objective, and also considers the service life of the electrochemical ES battery. An equipment replacement cost is added to the maintenance cost. The OF is calculated as presented in Equation (7) [20].

$$\min C = \min f_1 + \min C_i^m + \min C_{ca} \tag{7}$$

In Equation (7), C is the total cost, C_i is the replacement cost for equipment i, and C_{ca} is the tiered carbon trading cost. The equipment replacement cost is calculated as shown in Equation (8).

$$C_i = \sum_m \frac{cost_i N_i}{\gamma^m} \tag{8}$$

In Equation (8), $cost_i$ is the unit price of the equipment i, N_i is the total number of equipment i, γ is the discount factor, and m is the number of times the equipment needs to be replaced within the planning period. The calculation of the tiered carbon trading cost is shown in Equation (9) [21].

$$C_{ca} = \begin{cases} \varepsilon \cdot C_e, & C_e \le 2t' \\ \varepsilon \cdot 2t' + \varepsilon(1+\eta)(C_e - 2t'), & 2t' \le C_e \le 4t' \\ \varepsilon(2+\eta)2t' + \varepsilon(1+2\eta)(C_e - 4t'), & 4t' \le C_e \le 6t' \\ \varepsilon(3+3\eta)2t' + \varepsilon(1+3\eta)(C_e - 6t'), & 6t' \le C_e \le 8t' \\ \cdots & \end{cases} \tag{9}$$

In Equation (9), ε is the carbon trading price, C_e is the carbon trading volume, t' is the weight unit of the carbon trading (ton), and η is the carbon

trading price growth coefficient. The constraints of the hydrogen ES battery are shown in Equation (10) [22].

$$\begin{cases} S_{\min}^{t} \le S_t \le S_{\max}^{t} \\ P_1 \le P_{1,\max} \\ P_2 \le P_{2,\max} \end{cases} \tag{10}$$

In Equation (10), $S_{\min}^{t}$ is the min SOC of the hydrogen ES battery, $S_{\max}^{t}$ is the max SOC of the hydrogen ES battery, and S_t is the SOC of the hydrogen ES battery at time t. P_1 is the real-time power of the electrolyzer, $P_{1,\max}$ is the max power of the electrolyzer, P_2 is the real-time power of the fuel cell, and $P_{2,\max}$ is the max power of the fuel cell. The study uses the BAS-IMPSO algorithm to solve the model. First, the initial population is optimized using Logistic chaotic mapping [23]. Traditional PSO algorithms often use random generation when initializing the population, which makes it difficult to guarantee the uniformity of particle distribution and easily leads to the search process getting trapped in local optima. Introducing Logistic chaotic mapping can generate a more uniformly distributed random sequence within the interval $[0, 1]$, enhancing the diversity and ergodicity of the initial population. This helps the algorithm search more effectively in the global scope, thereby improving the CS and the quality of the solution set distribution. The expression of Logistic chaotic mapping is presented in Equation (11).

$$Z_{a,t''+1} = \nu Z_{a,t''}(1 - Z_{a,t''}) \tag{11}$$

In Equation (11), $Z_{a,t''+1}$ is the Logistic chaotic mapping of the variable a at the $t'' + 1$th iteration, and ν is the chaotic coefficient. A dynamic nonlinear inertial weight strategy is introduced to enable the algorithm to maintain a high weight in the early stage of the search to bolster the global exploration capacity, and to expedite the rate of weight decay during the later phase to strengthen the local fine-grained search. This mechanism helps the algorithm to boost the convergence accuracy and uniformity of the solution set distribution while avoiding premature convergence. Considering that the improved PSO algorithm performs better in group optimization, but is prone to getting trapped in local optima in high-dimensional space, while the BAS algorithm performs better in individual optimization [24]. Operational control issues demand rapid response and handling of continuous variables. The IMPSO exhibits favourable collective optimization efficiency but is prone to local optima. The BAS algorithm possesses highly effective individual directional search capabilities. The BAS-IMPSO hybrid optimizer, formed

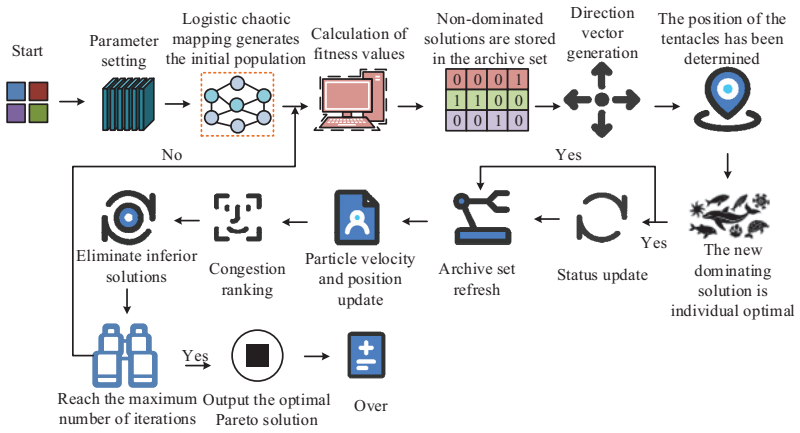

Figure 4 Detailed operational flow of the BAS-IMPSO algorithm.

by integrating both approaches, aims to balance global exploration with local exploitation, thereby enhancing optimization accuracy and speed under complex operational constraints. Therefore, the study integrates the two algorithms, retains the global optimization capability of the improved PSO algorithm, and combines the directional sensing characteristics of BAS to effectively enhance the local fine search and direction prediction capability of particles, thereby improving the CS and solution set quality of the algorithm. The BAS-IMPSO's operation flow is presented in Figure 4.

In Figure 4, an initial particle swarm with good distribution characteristics is generated using Logistic chaotic mapping, and the velocity vector and external archive set are initialized. The fitness of each particle is calculated to determine the individual optimal and global OSs, and non-dominated solutions that meet the conditions are stored in the archive set. A direction vector is randomly generated for each particle, and the positions of the "left and right tentacles" of the BAS algorithm are determined accordingly, and their fitness is evaluated to determine the search direction. If a new solution dominates the original individual OS, the particle state is updated, and the archive set is refreshed synchronously; otherwise, the particle velocity and position vectors are directly updated. Solutions in the archive set are sorted by congestion distance to eliminate inferior solutions. Upon reaching the maximum iteration count, the algorithm outputs the top 20% of solutions with the highest crowding degree in the archive as the final Pareto optimal solution set; otherwise, it returns to step 3 to continue iteration. The control strategy of the hybrid ES system in the DN is divided into three control modes based

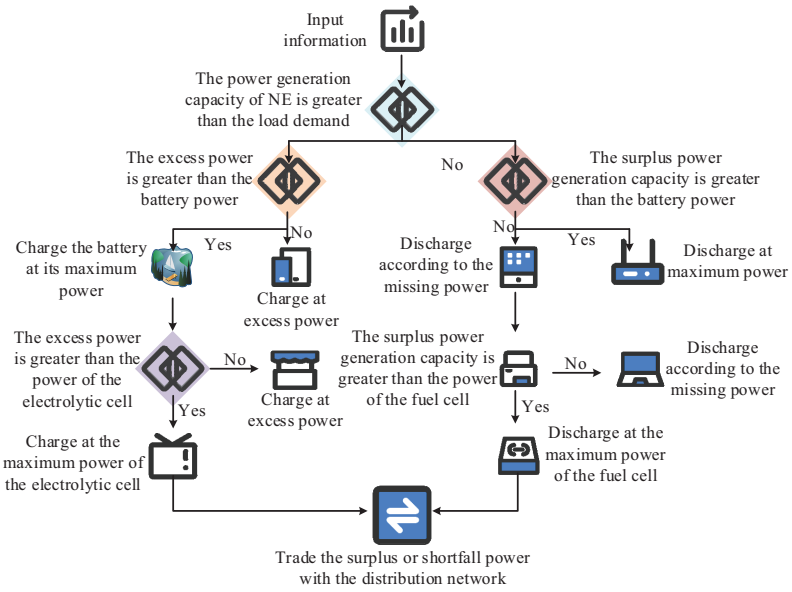

Figure 5 Control modes for hybrid ES systems in DNs.

on the difference between the system's PG and load demand, as presented in Figure 5.

In Figure 5, when there is a PG surplus, energy is consumed in the order of priority: batteries, hydrogen production through electrolysis, and electricity sold to the grid. When there is a PG deficit, the power gap is filled in the order of priority: batteries, fuel cells, and electricity purchased from the grid. When PG and load are balanced, all ES and conversion units are inactive. This strategy, with the ES system at its core, prioritizes internal consumption and ultimately achieves power balance through grid trading, thereby ensuring the system's low-carbon and efficient operation.

3 Analysis of Coordination Control Results of Hybrid ES System in DN

3.1 Analysis of Capacity Optimization Results of Hybrid ES System in DN

The experimental hardware setup included an Intel Core i9-12900K @ 3.2GHz processor, an NVIDIA RTX 3080 (12GB VRAM) graphics card, 64GB DDR4 3200MHz RAM, and 1TB NVMe SSD + 4TB HDD storage.

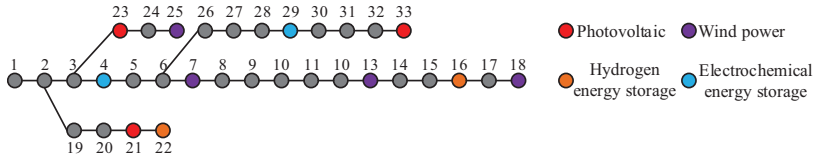

Figure 6 IEEE 33-node system.

The software setup used Windows 11 Professional as the operating system, MATLAB R2022a as the development platform, and the Simulink power system module library as the simulation tool. Programming was performed using MATLAB and Python 3.9. The CPA population size was set to 100, the max iteration count was 200, and the attraction rate, digestion rate, and prey escape rate were 0.8, 0.4, and 0.3, respectively. The daily load profile for the node system employed IEEE standard test data with a 10% random fluctuation overlay to simulate uncertainty. The simulation duration covered a typical day (24 hours) with a time resolution of one hour. The unit cost of lithium batteries was set at 1,500 yuan/kWh, while the unit power cost of hydrogen storage was set at 8,000 yuan/kW. Time-of-use electricity pricing followed industrial peak-off-peak tariff policies, with the carbon trading starting price set at 50 yuan/tonne. Case study simulations were conducted for validation within the IEEE 33 and IEEE 69 node systems, with the IEEE 33 node system structure depicted in Figure 6.

In Figure 6, the IEEE 33-node system incorporated three photovoltaic power generation systems with rated capacities of 0.8 MW, 1.2 MW, and 0.6 MW respectively. Four wind power generation systems were incorporated, with rated capacities of 1.0 MW, 0.8 MW, 1.5 MW, and 0.7 MW respectively. Two hydrogen storage units and two electrochemical storage devices were included, serving a typical residential and commercial mixed load profile. The system voltage reference was set at 12.66 kV, with a power reference of 1000 MW and a voltage scaling factor of 1.0 p.u. Figure 7 shows a comparison of the convergence performance of different algorithms.

In Figure 7(a), to verify the statistical significance of performance differences, each algorithm was independently run 30 times. The number of iterations required to converge to the optimal fitness value was recorded, and a paired t-test was conducted (significance level $\alpha = 0.05$). The results indicated that the differences in convergence iterations between the CPA and the NSGA-II, MOPSO, WOA, GA, and SA were statistically significant ($p < 0.01$). The CPA converged after 80 iterations, achieving a min fitness value of 0.022, which was 0.046, 0.023, and 0.057 lower than the

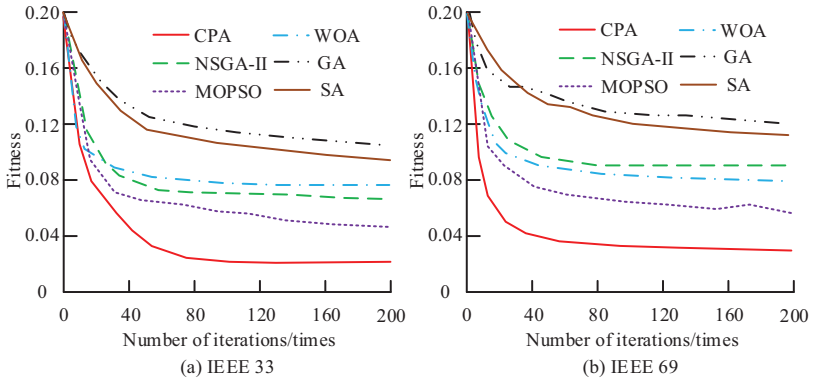

Figure 7 Comparison of convergence performance among different algorithms.

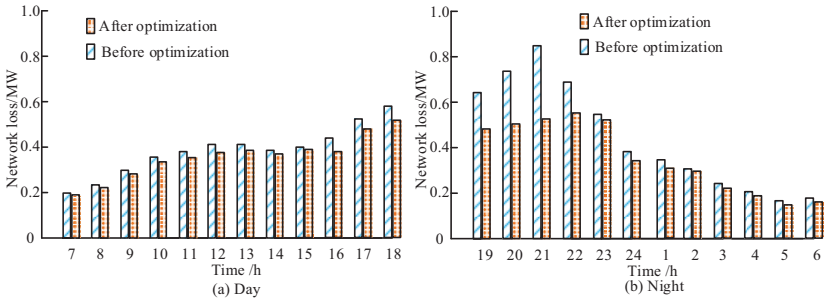

Figure 8 Network losses before and after the hybrid ES system in the DN.

NSGA-II, Multi-Objective PSO (MOPSO), and Whale Optimization Algorithm (WOA), respectively. The minimum fitness values for the standard GA and SA were 0.112 and 0.098 respectively, significantly higher than those achieved by the proposed CPA. The WOA, due to its uneven initial population distribution, prematurely fell into local optima. In Figure 7(b), in the IEEE 69-node system, the convergence capability of all four algorithms decreased. The optimal fitness value of the CPA increased by 0.013, which was 0.002 lower than the second-best performing MOPSO algorithm. The GA and SA increased by 0.013 and 0.010 respectively. Figure 8 shows the network loss situation before and after the hybrid ES system in the DN.

In Figure 8(a), the network loss of the DN first increased and then decreased over time, with the optimized network loss consistently lower than the unoptimized one. The average optimized network loss was 0.025 MW lower than the unoptimized one. In Figure 8(b), electricity consumption was

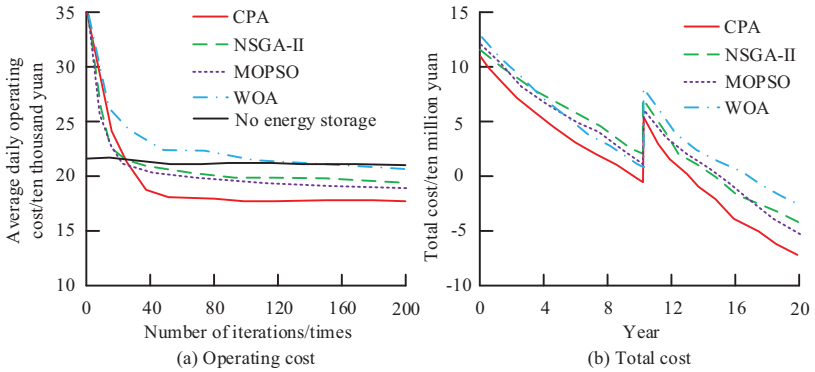

Figure 9 Comparison of system OCs without algorithms.

higher at night, and the network loss from 7 pm to 11 pm was much higher than other time periods, with the optimized network loss showing a more significant decrease. At 21 pm, the optimized network loss was 0.52 MW, which was 0.21 MW lower than the unoptimized one. The total network loss after optimization was 1.258 MW lower than the unoptimized one. The reduction in network losses was primarily attributable to the optimized scheduling of hybrid energy storage systems. During periods of low load demand or high renewable generation, the storage systems charged, absorbing local surplus power. This reduced the need for long-distance power transmission from the higher-level grid and the associated line losses. During peak load periods, the energy storage system discharged to support local demand, thereby reducing transmission currents on the lines. The optimization model coordinated the operation of the energy storage system to achieve a more rational distribution of power flow within the DN, consequently lowering overall joule losses. A comparison of system operating costs (OCs) under different algorithms is shown in Figure 9.

In Figure 9(a), the average daily OC of the hybrid ES system in the DN decreased continuously with the iteration count. The CPA achieved the min average daily OC of 1.754 million yuan, which was 79,000 yuan lower than the second-best MOPSO algorithm and 40,000 yuan lower than the average cost of the system without ES. In Figure 9(b), the CPA outperformed the other three algorithms in both initial investment cost and annual return. The initial investment cost was 108.2 million yuan, which was 3.05 million yuan lower than the second-best NSGA-II algorithm. The CPA had the fastest curve decline rate, resulting in higher annual returns and a recovery of all costs in 9.5 years. However, in the 10th year, due to the limitation of battery

cycle life, the total investment changed drastically after battery replacement. The total return of the CPA after 20 years was 72.36 million yuan.

3.2 Analysis of Operation Coordination Control Results of Hybrid ES System in DN

The experimental hardware and software settings were the same as in the first experiment. The particle swarm size of the improved PSO algorithm was set to 80, the max iteration count was 200, and the inertia weight range was [0.4, 0.9]. The tentacles length of the BAS algorithm was 0.1, and the search step size and step size decay factor were 0.05 and 0.95, respectively. The Pareto fronts of different algorithms are shown in Figure 10.

In Figure 10(a), the non-dominated solutions of the BAS-IMPSO algorithm were more evenly distributed and have higher frontier integrity. The non-dominated solutions of the CPA were mostly concentrated, with a few scores scattered around the perimeter. The OC of the DN was negatively correlated with carbon emission costs; higher OCs resulted in lower carbon emission costs and more stable voltage. Decision-makers need to make effective decisions between cost input and DN stability. In Figure 10(b), the non-dominated solutions of the IMPSO algorithm were randomly distributed, making it difficult to find the OS effectively. Figure 11 shows the load disturbance situation of the DN under different penetration rates (PRs).

In Figure 11(a), the load disturbance change of the BAS-IMPSO algorithm was relatively smooth, with a smaller disturbance amplitude. At node 20, the max load disturbance was 0.33 pu, which was 0.18 pu and 0.12 pu lower than the max disturbance values before optimization and the IMPSO algorithm, respectively. In Figure 11(b), the BAS-IMPSO algorithm had a better optimization effect on the 69-node system, with a smaller load

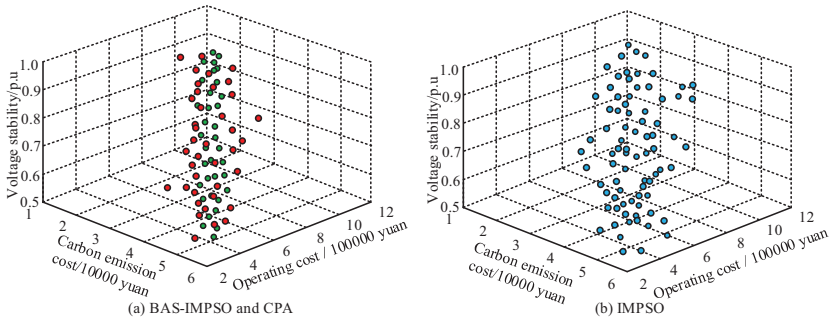

Figure 10 Pareto fronts for different algorithms.

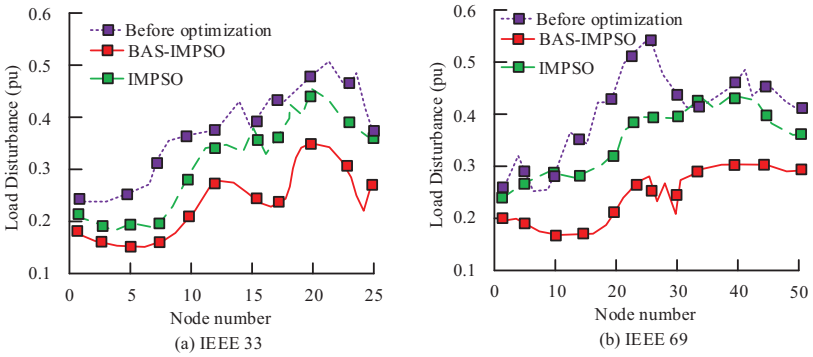

Figure 11 Load disturbance scenarios in DNs under different PRs.

Table 1 System OCs and voltage deviation at various load levels

Load Level (MW)	Algorithm Type	System OC (Ten Thousand Yuan)	Carbon Emission Cost (Ten Thousand Yuan)	Average Voltage Deviation (pu)
50	BAS-IMPSO	180.5	35.2	0.011
50	CPA	185.7	34.8	0.014
50	IMPSO	190.3	36.5	0.018
70	BAS-IMPSO	192.8	37.1	0.013
70	CPA	198.4	36.9	0.017
70	IMPSO	205.6	38.2	0.019
90	BAS-IMPSO	205.3	39.4	0.014
90	CPA	211.5	39	0.019
90	IMPSO	218.9	40.5	0.025

disturbance fluctuation amplitude. The max disturbance value was 0.30 pu, which was 0.24 pu lower than the max disturbance value before optimization. The system OC and voltage deviation under different load levels are presented in Table 1.

Table 1 shows that the BAS-IMPSO algorithm better balanced system OCs and carbon emission costs under different load levels, demonstrating superior overall performance. While both OCs and carbon emission costs increased with load levels, the relative advantage of the BAS-IMPSO algorithm remained significant. The average voltage deviation of the BAS-IMPSO algorithm at 90MW was 0.014, which was 0.005 and 0.011 pu lower than CPA and IMPSO, respectively. The reduction in operational costs stems from: (1) Peak-shaving and valley-filling revenue: Charging during off-peak electricity rates and discharging during peak periods to capture arbitrage

Table 2 Load disturbance suppression effect at different permeability values

Performance Indicators	PR 20%	PR 40%	PR 60%	PR 80%
Max Load Disturbance (pu)				
Before optimization	0.42	0.48	0.54	0.62
IMPSO	0.36	0.41	0.47	0.55
BAS-IMPSO	0.3	0.33	0.38	0.44
Voltage Qualification Rate (%)				
Before optimization	96.2	94.8	92.3	89.5
IMPSO	97.8	96.5	94.2	91.8
BAS-IMPSO	98.9	98.2	96.8	94.5
Network Loss (MW)				
Before optimization	2.85	3.12	3.45	3.81
IMPSO	2.63	2.87	3.18	3.49
BAS-IMPSO	2.41	2.64	2.92	3.21
Before optimization	0.12	0.15	0.16	0.18

opportunities. (2) Government subsidies: Incentive policies for energy storage discharge. (3) Tiered carbon trading mechanism: Optimized dispatch promotes local consumption of RE, reducing equivalent carbon emissions and thereby lowering carbon trading costs. (4) Equipment lifespan considerations: A full lifecycle model prevents overuse of storage equipment, delays replacement needs, and reduces long-term average annual costs. Table 2 shows the load disturbance suppression effect under different permeability rates.

Table 2 shows that the BAS-IMPSO algorithm exhibited the best load disturbance suppression effect under different RE PRs. At a PR of 40%, BAS-IMPSO suppressed the max load disturbance to 0.33 pu, which was 0.15 pu and 0.08 pu lower than the unoptimized version and the IMPSO algorithm, respectively. Under different PR scenarios, the system controlled by the BAS-IMPSO algorithm maintained the highest voltage qualification rate and the lowest network loss. Taking a 40% PR as an example, the voltage qualification rate reached 98.2%, and the network loss was 2.64 MW, a reduction of 0.48 MW compared to the unoptimized version. The results indicated that as the PR increased from 20% to 80%, the system stability challenge intensified, but the performance advantage of the BAS-IMPSO algorithm remained stable. The comparison of system performance under different device failure scenarios before and after optimisation is shown in Table 3.

In Table 3, the performance metrics of the BAS-IMPSO strategy significantly outperformed those of the uncoordinated control strategy and

Table 3 Comparison of system performance under different equipment failure scenarios before and after optimization

Fault Scenarios	Description	Control Strategy	Maximum Voltage Deviation (pu)	Average Voltage Compliance Rate (%)	Network Losses (MW)	Daily Operating Costs (¥10,000)
S0: Baseline Scenario	No faults, normal operation.	BAS-IMPSO	0.033	99.2	2.41	18.05
		IMPSO	0.041	98.1	2.63	19.03
		Uncoordinated control	0.058	95	2.85	20.56
S1: Single Energy Storage Failure	Sudden withdrawal of electrochemical energy storage at Node 7 (12:00-18:00).	BAS-IMPSO	0.048	98	2.59	18.98
		IMPSO	0.055	96.8	2.79	20.14
		Uncoordinated control	0.072	92.5	3.15	21.87
S2: Multiple Energy Storage Failures	Simultaneous failure of electrochemical energy storage at Node 7 and hydrogen storage electrolyser at Node 15 (14:00–20:00).	BAS-IMPSO	0.061	96.2	2.84	20.11
		IMPSO	0.073	94.1	3.08	21.55
		Uncoordinated control	0.095	88.3	3.62	23.74
S3: Critical Circuit Failure	Main trunk line (Node 2–3) disconnected, network topology altered (10:00–16:00).	BAS-IMPSO	0.052	97.3	2.71	19.42
		IMPSO	0.06	95.9	2.92	20.67
		Uncoordinated control	0.089	90.7	3.41	22.89
S4: Combined Failures	Simultaneous occurrence of S1 (energy storage fault) and S3 (line fault).	BAS-IMPSO	0.07	94.8	3.02	20.89
		IMPSO	0.085	92	3.31	22.45
		Uncoordinated control	0.112	85.4	3.98	24.68

demonstrated overall superiority over the IMPSO strategy. Under combined fault scenario S4, BAS-IMPSO maintained a voltage compliance rate of 94.8%, exceeding the uncoordinated control by 9.4 percentage points and reducing daily operational costs by approximately ¥37,900. This demonstrated that the joint coordinated control framework possessed online dynamic adjustment capabilities. Upon detecting equipment faults, it rapidly re-optimized the power commands for the remaining healthy equipment, effectively mitigating power deficits or abrupt power flow changes caused by faults. During fault periods, the system inevitably incurred increased network losses and operational costs to maintain stability. However, the BAS-IMPSO strategy minimized these costs through optimized dispatch. In Scenario S1, network losses increased by only 7.5% compared to normal conditions, significantly lower than the 30.7% increase observed without coordinated control strategies.

4 Conclusion

To tackle the problems of large load fluctuations and low voltage quality when NE sources are integrated into new DNs, a joint coordinated control method for hybrid ES systems in new DNs was proposed. Experiments showed that network losses in the DN initially increased and then decreased over time. After optimization, the average network loss was 0.025 MW lower than before optimization, and the total network loss was 1.258 MW lower. The CPA achieved the lowest average daily OC of 1.754 million yuan, which was 79,000 yuan lower than the second-best MOPSO algorithm and 40,000 yuan lower than the average cost of systems without ES. The initial investment cost of the CPA was 108.2 million yuan, which was 3.05 million yuan lower than the second-best NSGA-II algorithm, and all costs were recovered in 9.5 years. The BAS-IMPSO algorithm showed a more uniform distribution of non-dominated solutions and higher frontier integrity, while the CPA showed that most of the non-dominated solutions were concentrated, with a few scores spread over four weeks. The OC of the DN was negatively correlated with carbon emission costs; higher OCs resulted in lower carbon emission costs and more stable voltage. Decision-makers need to make effective decisions between cost input and DN stability. The BAS-IMPSO algorithm exhibited smaller load disturbance fluctuations, with a max disturbance value of 0.30 pu, which was 0.24 pu lower than the max disturbance value before optimization. The BAS-IMPSO algorithm demonstrated optimal load disturbance suppression performance under different RE PRs. At a 40%

PR, BAS-IMPSO suppressed the max load disturbance to 0.33 pu, which was 0.15 pu lower than the unoptimized algorithm and 0.08 pu lower than the IMPSO algorithm. The joint coordinated control framework could effectively improve the stability of the new DN and ensure power supply quality. This study still has some limitations, such as significant model fluctuations across different systems. Future research could incorporate the uncertainty of load forecasting and employ robust optimization methods to further enhance the strategy's anti-interference capability. The proposed joint coordinated control method incorporated stepwise carbon trading and equipment lifespan into its modelling framework. Its algorithm demonstrated favourable computational efficiency and held potential for practical engineering implementation. Annual operating costs were reduced by approximately ¥40,000, coupled with an investment payback period of around 9.5 years, demonstrating favourable economic benefits. This methodology could be integrated into DN energy management systems or distributed energy management platforms, providing dispatchers with a set of Pareto optimal solutions to assist decision-making between economic efficiency and power supply quality. Driven by the dual carbon goals, this approach holds clear application value for the planning and operation of DNs with high RE penetration.

References

[1] Qiu Y, Li Q, Ai Y, Chen W, Benbouzid M, Liu S, and Gao F. Two-stage distributionally robust optimization-based coordinated scheduling of integrated energy system with electricity-hydrogen hybrid energy storage[J]. Protection and Control of Modern Power Systems, 2023, 8(2): 1–14. DOI: 10.1186/s41601-023-00308-8.

[2] Grisales-Norena L F, Cortes-Caicedo B, Montoya O D, Gil-González W, and Muñoz J. Enhancing DC distribution network efficiency through optimal power coordination in lithium-ion batteries: A sparse nonlinear optimization approach[J]. Journal of Energy Storage, 2024, 96(1): 112484–112497. DOI: 10.1016/j.est.2024.112484.

[3] Li H, and He H. Learning to operate distribution networks with safe deep reinforcement learning[J]. IEEE Transactions on Smart Grid, 2022, 13(3): 1860–1872. DOI: 10.1109/tsg.2022.3142961.

[4] Islam M M, Yu T, Giannoccaro G, Mi Y, La Scala M, Nasab M R, and Wang J. Improving reliability and stability of the power systems: A comprehensive review on the role of energy storage systems to

enhance flexibility[J]. IEEE Access, 2024, 12(6): 152738–152765. DOI: 10.1109/access.2024.3476959.

[5] Ma Y, Hu Z, and Song Y. Hour-ahead optimization strategy for shared energy storage of renewable energy power stations to provide frequency regulation service[J]. IEEE Transactions on Sustainable Energy, 2022, 13(4): 2331–2342. DOI: 10.1109/tste.2022.3194718.

[6] Chen C, Li Y, Qiu W, Liu C, Zhang Q, Li Z,. . . and Yang L. Cooperative-game-based day-ahead scheduling of local integrated energy systems with shared energy storage[J]. IEEE Transactions on Sustainable Energy, 2022, 13(4): 1994–2011. DOI: 10.1109/tste.2022.3176613.

[7] Gu T, Wang P, Liang F, Xie G, Guo L, Zhang X P, and Shi F. Placement and capacity selection of battery energy storage system in the distributed generation integrated distribution network based on improved NSGA-II optimization[J]. Journal of Energy Storage, 2022, 52(4): 104716–104732. DOI: 10.1016/j.est.2022.104716.

[8] Liu K, Sheng W, Li Z, Liu F, Liu Q, Huang Y, and Li Y. An energy optimal schedule method for distribution network considering the access of distributed generation and energy storage[J]. IET Generation, Transmission and Distribution, 2023, 17(13): 2996–3015. DOI: 10.1049/gtd2.12855.

[9] Shafiei K, Zadeh S G, and Hagh M T. Planning for a network system with renewable resources and battery energy storage, focused on enhancing resilience[J]. Journal of Energy Storage, 2024, 87(4): 111339–111352. DOI: 10.1016/j.est.2024.111339.

[10] Piltan G, Pirouzi S, Azarhooshang A, Jordehi A R, Paeizi A, and Ghadamyari M. Storage-integrated virtual power plants for resiliency enhancement of smart distribution systems[J]. Journal of Energy Storage, 2022, 55(9): 105563–105576. DOI: 10.1016/j.est.2022.105563.

[11] Abid M S, Apon H J, Morshed K A, and Ahmed A. Optimal planning of multiple renewable energy-integrated distribution system with uncertainties using artificial hummingbird algorithm[J]. IEEE Access, 2022, 10(2): 40716–40730. DOI: 10.1109/access.2022.3167395.

[12] Zadehbagheri M, Dehghan M, Kiani M, and Pirouzi S. Resiliency-constrained placement and sizing of virtual power plants in the distribution network considering extreme weather events[J]. Electrical Engineering, 2025, 107(2): 2089–2105. DOI: 10.1007/s00202-024-02583-6.

[13] Pompern N, Premrudeepreechacharn S, Siritaratiwat A, and Khunkitti S. Optimal placement and capacity of battery energy storage system in distribution networks integrated with PV and EVs using metaheuristic algorithms[J]. IEEE Access, 2023, 11(5): 68379–68394. DOI: 10.1109/ACCESS.2023.3291590.

[14] Levin T, Bistline J, Sioshansi R, Cole W J, Kwon J, Burger S P,... and Botterud A. Energy storage solutions to decarbonize electricity through enhanced capacity expansion modelling[J]. Nature Energy, 2023, 8(11): 1199–1208. DOI: 10.1038/s41560-023-01340-6.

[15] Zheng X, Khodayar M E, Wang J, Yue M, and Zhou A. Distributionally robust multistage dispatch with discrete recourse of energy storage systems[J]. IEEE Transactions on Power Systems, 2024, 39(6): 6960–6973. DOI: 10.1109/tpwrs.2024.3369664.

[16] Su Y, and Teh J. Two-stage optimal dispatching of AC/DC hybrid active distribution systems considering network flexibility[J]. Journal of Modern Power Systems and Clean Energy, 2022, 11(1): 52–65. DOI: 10.35833/mpce.2022.000424.

[17] Hamidan M A, and Borousan F. Optimal planning of distributed generation and battery energy storage systems simultaneously in distribution networks for loss reduction and reliability improvement[J]. Journal of Energy Storage, 2022, 46(8): 103844–103859. DOI: 10.1016/j.est.2021.103844.

[18] Yuvaraj T, Devabalaji K R, Kumar J A, Thanikanti S B, and Nwulu N I. A comprehensive review and analysis of the allocation of electric vehicle charging stations in distribution networks[J]. IEEE Access, 2024, 12(6): 5404–5461. DOI: 10.1109/access.2023.3349274.

[19] Boroumandfar G, Khajehzadeh A, Eslami M, and Syah R B. Information gap decision theory with risk aversion strategy for robust planning of hybrid photovoltaic/wind/battery storage system in distribution networks considering uncertainty. Energy, 2023, 278(4): 127778–127790. DOI: 10.1016/j.energy.2023.127778.

[20] Jiang X, Zhou Y, Ming W, Yang P, and Wu J. An overview of soft open points in electricity distribution networks[J]. IEEE Transactions on Smart Grid, 2022, 13(3): 1899–1910. DOI: 10.1109/TSG.2022.3148599.

[21] Babu B S. Adaptive dragonfly optimization based placement of capacitor banks for voltage stability enhancement in distribution networks[J]. Strategic Planning for Energy and the Environment, 2021, 5(7): 25–38. DOI: 10.13052/spee1048-5236.4012.

[22] Aliabadi M J and Radmehr M. Hybrid energy system optimization integrated with battery storage in radial distribution networks considering reliability and a robust framework. Scientific Reports, 2024, 14(1): 26597–26615. DOI: 10.1038/s41598-024-73808-8.

[23] Wang H, Zhang Z, and Gao N. Design of renewable energy consumption scheduling model based on quantitative feedback theory[J]. Strategic Planning for Energy and the Environment, 2023, 2(9): 57–78. DOI: 10.13052/spee1048-5236.4214.

[24] Xu X, Li Y, Yan Z, Ma H, and Shahidehpour M. Hierarchical central-local inverter-based voltage control in distribution networks considering stochastic PV power admissible range[J]. IEEE Transactions on Smart Grid, 2022, 14(3), 1868–1879. DOI: 10.1109/tsg.2022.3213776.

Biographies

Hao Bai (July 1987–), male, graduated from Huazhong University of Science and Technology with a PhD in Electrical Engineering. After graduation, I worked as a senior engineer at Southern Power Grid Science Research Institute Co., Ltd. My current research direction is engaged in the planning and operation of distribution networks.

Qingsheng Li (June 1971–), male, graduated from Guizhou Institute of Technology with a Bachelor's degree in Electrical Engineering. After graduation, I worked as a professor level senior engineer in a subsidiary company. My current research direction is engaged in the simulation of new energy storage, distribution networks, and power systems.

Yuxin Wen (March 1999–), male, graduated from Wuhan University with a master's degree in Electrical Engineering. After graduation, I worked as an engineer at Southern Power Grid Science Research Institute Co., Ltd. My current research direction is engaged in the operation and simulation of distribution networks.

Yipeng Liu (October 1998–), male, graduated from Wuhan University with a master's degree in Electrical Engineering. After graduation, I worked as an engineer at Southern Power Grid Science Research Institute Co., Ltd. My current research direction is engaged in the operation and simulation of distribution networks.